Mon. Not. R. Astron. Soc. **342,** 1131–1138 (2003)

Optical flashes and very early afterglows in wind environments

X. F. Wu,[1⋆] Z. G. Dai,[1⋆] Y. F. Huang[1,2⋆] and T. Lu[1,2⋆]

[1]*Department of Astronomy, Nanjing University, Nanjing 210093, China*
[2]*LCRHEA, Institute for High-Energy Physics, Chinese Academy of Sciences, Beijing 100039, China*

Accepted 2003 March 6. Received 2003 March 4; in original form 2002 June 21

ABSTRACT

The interaction of a relativistic fireball with its ambient medium is described through two shocks: a reverse shock that propagates into the fireball, and a forward shock that propagates into the medium. The observed optical flash of GRB 990123 has been considered to be the emission from such a reverse shock. The observational properties of afterglows suggest that the progenitors of some γ-ray bursts (GRBs) may be massive stars and their surrounding media may be stellar winds. We here study very early afterglows from the reverse and forward shocks in winds. An optical flash mainly arises from the relativistic reverse shock, while a radio flare is produced by the forward shock. The peak flux densities of optical flashes are larger than 1 Jy for typical parameters, if we do not take into account some appropriate dust obscuration along the line of sight. The radio flare always has a long-lasting constant flux, which will not be covered up by interstellar scintillation. The non-detections of optical flashes brighter than about ninth magnitude may constrain the GRB isotropic energies to be no more than a few 10^{52} erg and wind intensities to be relatively weak.

Key words: hydrodynamics – relativity – shock waves – gamma-rays: bursts.

1 INTRODUCTION

Gamma-ray bursts (GRBs) have been well understood since the discovery of afterglows in 1997 (Wijers, Rees & Mészáros 1997; Piran 1999; van Paradijs, Kouveliotou & Wijers 2000; Mészáros 2002). The hydrodynamic evolution of a GRB remnant is well described by an ultrarelativistic forward shock that sweeps into the interstellar medium (ISM) and slows down to the non-relativistic phase, while the resulting afterglow is due to synchrotron radiation of electrons accelerated by the shock.

However, emission from a reverse shock propagating into the shell of the GRB ejecta has also been predicted (Mészáros & Rees 1997; Sari & Piran 1999a). Before the reverse shock crosses the shell, the shocked shell matter carries an amount of energy comparable to that of the forward shocked interstellar medium. The prompt optical flash of GRB 990123 (Akerlof et al. 1999) has motivated investigations of emission from the reverse shock (Mészáros & Rees 1999; Sari & Piran 1999b; Kobayashi & Sari 2000; Kobayashi 2000). The light curve of an optical flash in a uniform ISM has been well studied in both thin-shell and thick-shell cases (Kobayashi 2000), and it is found that the optical flash of GRB 990123 is due to radiation from a mildly relativistic reverse shock (Kobayashi & Sari 2000). Recently, the contribution of reverse shocks to early radio afterglows was also discussed by Soderberg & Ramirez-Ruiz (2002a,b).

⋆E-mail: xfwu@nju.edu.cn (XFW); daizigao@public1.ptt.js.cn (ZGD); hyf@nju.edu.cn (YFH); tlu@nju.edu.cn (TL)

There is increasing evidence for the association between some GRBs and Type Ib/c supernovae. The most direct evidence is the association of GRB 980425 with SN 1998bw (Galama et al. 1998). This association is strengthened by its radio emission after the burst (Li & Chevalier 1999). Up to now several GRB afterglows, e.g. GRB 970228 (Reichart 1999), 970508 (Sokolov 2001), 980326 (Bloom et al. 1999), 990712 (Sahu et al. 2000), 991208 (Castro-Tirado et al. 2001), 000911 (Lazzati et al. 2001) and 011211 (Bloom et al. 2002), have shown a supernova component in their light curves peaking at $t_\oplus = (1+z)t_{\rm SN,peak}$, with $t_{\rm SN,peak} \sim 15$ d for SNIc. One of the most popular central engines of GRBs is now believed to be the collapse of massive stars (Woosley 1993; Paczyński 1998). This collapsar/hypernova scenario naturally explains the broad and shifted iron-group emission lines in GRBs (McLaughlin et al. 2002). In the envelope models the iron line emission can be attributed either to the irradiated shallower layers on the funnel wall along the rotation axis by a continuing but decaying relativistic outflow (Rees & Mészáros 2000) or to the dissipation of the magnetized thermal bubble expanding into the H envelope of the progenitor, which results from the interaction between the jet with continuing energy injection and the stellar envelope (Mészáros & Rees 2001). The place of iron line emission in the envelope models is at the H envelope radius $r \sim 10^{13}$ cm, where a small amount of iron, $\sim 10^{-8}$ $M_\odot$ to $\sim 10^{-5}$ $M_\odot$, can meet the requirement. Other iron line emission models require a large line emission radius, $r \sim 10^{16}$ cm, and much larger iron mass $\geqslant 0.06$ $M_\odot$ (Vietri et al. 2001; Böttcher & Fryer 2001). The measured emission lines in the X-ray afterglow of GRB 011211 favour the latter (Reeves et al. 2002). The

pre-explosion wind structure can survive in envelope models but may be destroyed in other models due either to the ejection of SN prior to GRB or to the common envelope evolution in the binary system. Detailed calculations and more sensitive data on X-ray afterglow spectral features will distinguish between the various line emission models (Ballantyne & Ramirez-Ruiz 2001).

The light-curve steepening of some well-observed GRB afterglows deviates from the predictions of the standard model (Sari, Piran & Narayan 1998). This deviation leads to discussions of the environment and geometry effects. Previous studies have discussed the afterglow from a spherical blast wave in a wind (Dai & Lu 1998; Chevalier & Li 1999, 2000) and from a jet in a wind (Livio & Waxman 2000; Dai & Gou 2001; Gou et al. 2001). The wind environments of GRB 970228, 970508, 991216 and 000301c are recognized in the spherical-wind model (Chevalier & Li 2000; Li & Chevalier 2001). In the jet model, 10 broad-band GRB afterglows (i.e. GRB 970508, 980519, 990123, 990510, 991208, 991216, 000301c, 000418, 000926 and 010222) have been well fitted (Panaitescu 2001; Panaitescu & Kumar 2001, 2002). Among them, only GRB 980519, 990123 and 990510 are inconsistent with wind environments. However, we also noticed that Frail et al. (2000) gave a better fit for their first 63 d of observations of the radio afterglow of GRB 980519 in the spherical-wind model.

Information on the surrounding environment of a GRB can also be obtained by considering the evolution of the soft X-ray absorption property according to the surrounding density distribution (Lazzati & Perna 2002). The expected absorption of a wind environment will quickly drop to an undetectable level in no more than 1 s. This conflicts with the evidence of variable soft X-ray absorption in three GRBs detected by *BeppoSAX*. None the less, the wind environments cannot be excluded by this method due to the limited samples. It may give some evidence for another type of GRB environment, such as dense clouds. Superbubbles, which are proposed as the sites of GRBs, have been expected to explain the obtained low densities $n \sim 10^{-3}$ cm^{-3} (Scalo & Wheeler 2001). It requires a very weak stellar wind at least six orders weaker than that of the progenitor of SN 1998bw to ensure non-contamination of the superbubble by the wind at a typical afterglow radius. The wind profile $n \propto r^{-2}$ may be terminated at some radius $r \sim 10^{17}$ cm, where the wind sweeps up a mass of ISM comparable to that of the wind and leads to a quasi-homogeneous dense shell with the mean density $\sim 10^2$–10^3 cm^{-3} and thickness $\sim 10^{17}$ cm (Ramirez-Ruiz et al. 2001). This termination of the wind profile will not affect our analysis of the dynamic evolution of very early afterglows, but has the potential reduction of the optical flash. In this paper we perform a more detailed calculation of the very early afterglows of GRBs in wind environments including the reverse shock effect. In Section 2 we give the hydrodynamics of forward and reverse shocks. In Section 3 early afterglow light curves at optical and radio bands are calculated. We discuss some observational implications of our results in Section 4. The synchrotron self-absorption of electrons with a broken power-law energy distribution is discussed in the Appendix.

2 HYDRODYNAMICS OF FORWARD AND REVERSE SHOCKS

We consider a uniform and cold relativistic coasting shell with rest mass M_0, energy E, initial Lorentz factor $\eta = E/M_0 c^2$ and observed width Δ, which sweeps up a wind with particle number density $n_1 = Ar^{-k}$ ($k = 2$), where (Chevalier & Li 1999, 2000)

$$A = \dot{M}/4\pi m_{\rm p} v_{\rm w} = 3 \times 10^{35} A_* \,{\rm cm}^{-1}$$

and

$$A_* = (\dot{M}/10^{-5}\,{\rm M}_\odot\,{\rm yr}^{-1})(v_{\rm w}/10^3\,{\rm km\,s}^{-1})^{-1}.$$

Two shocks develop: a forward shock propagating into the wind, and a reverse shock propagating into the shell. There are four regions separated by the two shocks: (1) the unshocked wind, (2) the shocked wind, (3) the shocked shell material, (4) the unshocked shell material. From the shock jump conditions and equality of pressures and velocities along the contact discontinuity, the Lorentz factor γ, pressure p and number density n in both shocked regions can be determined by n_1, n_4 and η (Blandford & McKee 1976, hereafter BM).

We define the Sedov radius, at which the swept-up wind's rest-mass energy equals the initial energy E of the shell, i.e. $l = M_0\eta/(4\pi A m_{\rm p})$. Assuming that the shell does not enter the spreading stage, the width Δ is a constant, and $n_4 = M_0/(4\pi\, m_{\rm p}\, r^2\, \Delta\, \eta) \propto r^{-2}$. The property of the reverse shock is largely determined by a parameter defined as $f = n_4/n_1$ (Sari & Piran 1995), which can be further given by

$$f = \frac{l}{\Delta\eta^2}. \tag{1}$$

As shown by Sari & Piran (1995), if $f \gg \eta^2$, or the baryon loading $M_0 \gg 4\pi\, m_{\rm p}\, A\, \Delta\, \eta^3$, the reverse shock will be a Newtonian reverse shock (NRS); and if $f \ll \eta^2$, or $M_0 \ll 4\pi\, m_{\rm p}\, A\, \Delta\, \eta^3$, the reverse shock will be a relativistic reverse shock (RRS). For RRS, the Lorentz factor of the shocked shell relative to the unshocked shell is $\overline{\gamma}_3 = \eta^{1/2} f^{-1/4}/\sqrt{2}$, and the Lorentz factors of shocked matter are $\gamma_2 = \gamma_3 = \eta^{1/2} f^{1/4}/\sqrt{2}$. The time for the reverse shock to cross the shell in the fixed frame is

$$t_\Delta = \frac{\alpha \Delta \eta f^{1/2}}{c}, \tag{2}$$

where $\alpha = 1/2$ for RRS and $\alpha = 3/\sqrt{14}$ for NRS (Sari & Piran 1995). The shock expands to the radius $R_\Delta \approx ct_\Delta = \alpha\sqrt{l\Delta}$ when the reverse shock is just over. In addition to R_Δ there are two other characteristic radii involved here: the deceleration radius $R_\eta = l\,\eta^{-2}$, at which the swept-up mass is M_0/η, and the shell spreading radius $R_{\rm s} = \Delta\,\eta^2$. They have different dependences on l, Δ and η for the wind and ISM cases (Sari & Piran 1995). A parameter $\zeta = \eta^{-2}\sqrt{l/\Delta}$ is introduced to compare these three radii. According to equation (1), we get

$$R_\eta = \zeta R_\Delta/\alpha = \zeta^2 R_{\rm s}, \tag{3}$$

with $f = \zeta^2\eta^2$. The value $\zeta \ll 1$ describes RRS: $f \ll \eta^2$, and $R_\eta \ll R_\Delta \ll R_{\rm s}$; while $\zeta \gg 1$ describes NRS: $f \gg \eta^2$, and $R_{\rm s} \ll R_\Delta \ll R_\eta$. For RRS, the previous assumption of $\Delta = $ const is always satisfied, and deceleration of the shell happens before the reverse shock crosses it. For NRS, we must consider the spreading effect of the shell, and $\Delta = r/\eta^2$ with $n_4 = Al/r^3$. The comoving density ratio $f = l/r$ decreases with increasing r. The reverse shock becomes transrelativistic at $R_{\rm N} = l/\eta^2 (= R_\eta)$ when $f = \eta^2$. A similar correction must be made to t_Δ and R_Δ since Δ and f vary with r. We are most interested in RRS because of both a large energy output and a constant width.

Before RRS crosses the shell, the distance that the shell travels when RRS crosses a length dx in the unshocked shell frame can be given by (Kobayashi 2000)

$$\mathrm{d}r = \alpha\eta\sqrt{f}\,\mathrm{d}x. \tag{4}$$

The shocked electron number is proportional to x/Δ. In the observer's frame we have $r = 2c\gamma_3^2 t_\oplus$, so the hydrodynamic variables are

$$n_3 = \frac{8\sqrt{2}A}{\eta l^{1/4}\Delta^{7/4}}\left(\frac{t_\oplus}{T}\right)^{-2}, \quad e_3 = \frac{8Am_{\rm p}c^2}{l^{1/2}\Delta^{3/2}}\left(\frac{t_\oplus}{T}\right)^{-2}, \tag{5}$$

$$\gamma_3 = \frac{1}{\sqrt{2}}\left(\frac{l}{\Delta}\right)^{1/4}, \qquad N_{\rm e} = N_0\frac{t_\oplus}{T}, \tag{6}$$

where $N_0 = M_0/m_{\rm p}$ is the total electron number of the shell and $T = \Delta/(2c)$ is the observer's time at which the RRS crosses the shell, which is one-half of the crossing time adopted by Kobayashi (2000).

After RRS crosses the shell, the temperature of the shocked shell is very high and it will expand adiabatically and enter the spreading stage. Since it is located not far away from the forward shocked wind, we take the BM self-similar adiabatic solution with impulsive energy injection for the evolution of the shocked shell (Kobayashi & Sari 2000). With $p_3 \propto n_3^{4/3}$, we get $p_3 \propto r^{(4k-26)/3} \propto r^{-6}$, $\gamma_3 \propto r^{(2k-7)/2} \propto r^{-3/2}$, $n_3 \propto r^{(2k-13)/2} \propto r^{-9/2}$ and $r \propto t^{1/4}{}_\oplus$. The hydrodynamic variables are therefore given by

$$n_3 = n_3(T)\left(\frac{t_\oplus}{T}\right)^{-9/8}, \qquad e_3 = e_3(T)\left(\frac{t_\oplus}{T}\right)^{-3/2}, \tag{7}$$

$$\gamma_3 = \gamma_3(T)\left(\frac{t_\oplus}{T}\right)^{-3/8}, \qquad N_{\rm e} = N_0. \tag{8}$$

The hydrodynamic evolution of a relativistic forward shock in a wind has already been discussed in some detail (Dai & Lu 1998; Chevalier & Li 2000; Panaitescu & Kumar 2000). Before RRS crosses the shell, the Lorentz factor of the forward shock $\gamma_{\rm sh} = \sqrt{2}\gamma_2$ is a constant and equals $\sqrt{2}\gamma_3$. The forward shock radius is $r = 2\gamma^2{}_{\rm sh}\, ct_\oplus = 4\gamma^2_{2ct\oplus}$. Note that there is a difference of a factor of 2 between the reverse shock radius and the forward shock radius, which arises from the fact that the forward shock moves with $\gamma_{\rm sh}$ at any time although the photon emitter travels with γ_2 (Chevalier & Li 2000). So the time when the reverse shock is finished becomes $T' = T/2$.

For $t_\oplus \leqslant T'$ the hydrodynamic variables evolve as

$$n_2 = \frac{8\sqrt{2}A}{l^{3/4}\Delta^{5/4}}\left(\frac{t_\oplus}{T'}\right)^{-2}, \qquad e_2 = \frac{8Am_{\rm p}c^2}{l^{1/2}\Delta^{3/2}}\left(\frac{t_\oplus}{T'}\right)^{-2}, \tag{9}$$

with

$$\gamma_2 = \sqrt{2}(l/\Delta)^{1/4}/2.$$

For $t_\oplus > T'$, the hydrodynamic variables evolve as

$$n_2 = n_2(T')\left(\frac{t_\oplus}{T'}\right)^{-5/4}, \qquad e_2 = e_2(T')\left(\frac{t_\oplus}{T'}\right)^{-3/2}, \tag{10}$$

with

$$\gamma_2 = \gamma_2(T')(t_\oplus/T')^{-1/4}.$$

The above analytical hydrodynamic evolution for both the reverse shock and forward shock is valid only in the relativistic phase. However, a late-time afterglow may be produced by a non-relativistic forward shock (Huang, Dai & Lu 1998; Huang, Dai & Lu 1999, 2000). Thus, our results are applied only for early or very early afterglows in wind environments, including the reverse shock emission.

3 LIGHT CURVE OF VERY EARLY AFTERGLOW

3.1 Radiation from RRS

The shock accelerates electrons to a power-law energy distribution with an index p and with a minimum Lorentz factor $\gamma_{\rm m} = \xi_{\rm e}(\overline{\gamma}_3 - 1)[(p-2)/(p-1)]m_{\rm p}/m_{\rm e}$, where $\xi_{\rm e}$ is the fraction of the internal energy density carried by the electrons. The standard radiation mechanism for GRB afterglows is synchrotron radiation by relativistic electrons in the magnetic field whose energy density is another fraction (ξ_B) of the internal energy density. We also consider synchrotron self-absorption at the radio band. Thus, the spectrum as discussed by Sari et al. (1998) in the ISM case can be used to discuss an afterglow in the wind case. The spectrum is characterized by three break frequencies: the typical frequency $\nu_{\rm m}$, the cooling frequency $\nu_{\rm c}$, and the self-absorption frequency $\nu_{\rm a}$. A detailed derivation of $\nu_{\rm a}$ for fast-cooling and slow-cooling regimes is given in the Appendix. Since $B \propto (\xi_B n_1)^{1/2}\gamma_3$ and $\gamma_{\rm c} \propto 1/(\gamma_3 B^2 t_\oplus)$, we have $\nu_{\rm m} \propto \gamma_3\, \gamma^2{}_{\rm m} B$ and $\nu_{\rm c} \propto \gamma_3\, \gamma^2{}_{\rm c} B$. The peak flux $F_{\nu,\max} \propto N_{\rm e}\, \gamma_3 B/D^2$, where D is the distance from the GRB site to the observer.

Before RRS crosses the shell ($t_\oplus \leqslant T$),

$$\nu_{\rm m} = 8.65\times10^{16}E_{52}^{-1/2}\xi_{\rm e,0}^2\xi_{B,-2}^{1/2}\eta_{300}^2A_*\Delta_{13}^{-1/2}\left(\frac{t_\oplus}{T}\right)^{-1}\ {\rm Hz}, \tag{11}$$

$$\nu_{\rm c} = 1.32\times10^{12}E_{52}^{1/2}\xi_{B,-2}^{-3/2}A_*^{-2}\Delta_{13}^{1/2}\frac{t_\oplus}{T}\ {\rm Hz}, \tag{12}$$

$$F_{\nu,\max}^{\rm rs} = 1.42E_{52}\xi_{B,-2}^{1/2}\eta_{300}^{-1}A_*^{1/2}\Delta_{13}^{-1}D_{28}^{-2}\ {\rm Jy}, \tag{13}$$

where $E = 10^{52}E_{52}$ erg, $\eta = 300\eta_{300}$, $\Delta = 10^{13}\Delta_{13}$ cm, $\xi_B = 10^{-2}\xi_{B,-2}$, $\xi_{\rm e} = 0.6\xi_{\rm e,0}$, $A = 3\times10^{35}A_*$ cm^{-1} and $D = 10^{28}D_{28}$ cm. The time for the reverse shock to cross the shell is $T = 167\Delta_{13}$ s. For $\nu_{\rm c} \leqslant \nu_{\rm a} \leqslant \nu_{\rm m}$, we have

$$\nu_{\rm a} = 4.11\times10^{13}E_{52}^{1/6}\eta_{300}^{-1/3}A_*^{1/6}\Delta_{13}^{-5/6}\left(\frac{t_\oplus}{T}\right)^{-2/3}\ {\rm Hz}, \tag{14}$$

which is consistent with equation (18) of Dai & Lu (2001). For $\nu_{\rm a} \leqslant \nu_{\rm c} \leqslant \nu_{\rm m}$, we have

$$\nu_{\rm a} = 6.47\times10^{14}E_{52}^{-1/10}\eta_{300}^{-3/5}A_*^{19/10}\Delta_{13}^{-19/10}\xi_{B,-2}^{6/5}\left(\frac{t_\oplus}{T}\right)^{-2}\ {\rm Hz}. \tag{15}$$

The cooling Lorentz factor ($\gamma_{\rm c} \propto t_\oplus/T$) is determined by the dynamical time-scale. At very early times, $\gamma_{\rm c}$ may be less than unity, which is impossible in physics. In fact the radiation power of such electrons with $\gamma_{\rm c} \simeq 1$ will be cyclotron power, instead of synchrotron power. According to Dai & Lu (2001), we neglect the radiation before $t_{\oplus,\rm crit}$ (same as t_0 in Dai & Lu 2001) when $\gamma_{\rm c} = 1$,

$$t_{\oplus,\rm crit} = 11.3E_{52}^{-1/4}\Delta_{13}^{1/4}\xi_{B,-2}A_*^{5/4}{\rm s}, \tag{16}$$

which is the beginning for our calculation.

When RRS crosses the shell ($t_\oplus > T$), the shock-accelerated electrons will be in the slow-cooling regime if $\nu_{\rm c}\ (T) > \nu_{\rm m}\ (T)$. However, there will be no radiation if $\nu_{\rm c}\ (T) < \nu_{\rm m}\ (T)$, because all the previously shocked electrons have cooled and no newly shocked electrons are in the shell when $t_\oplus > T$. The break frequencies and peak flux for $\nu_{\rm c}\ (T) > \nu_{\rm m}\ (T)$ are

$$\begin{aligned}
\nu_{\rm m} &= \nu_{\rm m}(T)\left(\frac{t_\oplus}{T}\right)^{-15/8},\\
\nu_{\rm cut} &= \nu_{\rm c}(T)\left(\frac{t_\oplus}{T}\right)^{-15/8},\\
F_{\nu,\max} &= F_{\nu,\max}(T)\left(\frac{t_\oplus}{T}\right)^{-9/8}.
\end{aligned} \tag{17}$$

We have also derived the self-absorption frequency: in the slow-cooling phase, $\nu_{\rm a} \propto (t_\oplus/T)^{-3/5}$ for $\nu_{\rm a} \leqslant \nu_{\rm m} \leqslant \nu_{\rm cut}$, and $\nu_{\rm a} \propto (t_\oplus/T)^{-(15p+26)/8(p+4)}$ for $\nu_{\rm m} \leqslant \nu_{\rm a} \leqslant \nu_{\rm cut}$. The time for the reverse shocked shell to become non-relativistic, i.e. when $\gamma_3 = 2$, is

$$t_{\oplus,\rm nr} = 197.0 E_{52}^{2/3} A_*^{-2/3} \Delta_{13}^{-2/3} T. \quad (18)$$

3.2 Radiation from the forward shock

Before RRS crosses the shell, the forward shocked wind matter moves with the same Lorentz factor as the reverse shocked shell matter. Most of the initial kinetic energy of the shell has been transferred to the forward shocked matter, as shown in equation (3). The forward shock decelerates at a slower rate than the shocked shell does after the crossing time. We can consider the shocked shell as a tail of the forward shock based on the BM solution with its self-similar parameter $\chi \propto r^{4-k} \propto r^2$, which describes inward motion of the shocked shell relative to the shock front as the shock radius increases.

Before RRS crosses the shell ($t_\oplus \leqslant T'$), the radiation from the forward shock can be described by

$$\nu_{\rm m} = 1.70 \times 10^{17} E_{52}^{1/2} \xi_{\rm e,0}^2 \xi_{B,-2}^{1/2} \Delta_{13}^{-3/2} \left(\frac{t_\oplus}{T'}\right)^{-1} \text{Hz}, \quad (19)$$

$$\nu_{\rm c} = 5.28 \times 10^{12} E_{52}^{1/2} \xi_{B,-2}^{-3/2} A_*^{-2} \Delta_{13}^{1/2} \frac{t_\oplus}{T'} \text{Hz}, \quad (20)$$

$$F_{\nu,\rm max}^{\rm fs} = 5.07 E_{52}^{1/2} A_* \Delta_{13}^{-1/2} D_{28}^{-2} \text{Jy}. \quad (21)$$

For $\nu_{\rm c} \leqslant \nu_{\rm a} \leqslant \nu_{\rm m}$, we have the self-absorption frequency

$$\nu_{\rm a} = 2.92 \times 10^{13} A_*^{1/3} \Delta_{13}^{-2/3} \left(\frac{t_\oplus}{T'}\right)^{-2/3} \text{Hz}, \quad (22)$$

and for $\nu_{\rm a} \leqslant \nu_{\rm c} \leqslant \nu_{\rm m}$ we have

$$\nu_{\rm a} = 9.78 \times 10^{13} E_{52}^{-2/5} A_*^{11/5} \Delta_{13}^{-8/5} \xi_{B,-2}^{6/5} \left(\frac{t_\oplus}{T'}\right)^{-2} \text{Hz}. \quad (23)$$

The time for $\gamma_{\rm c} \geqslant 1$ is

$$t'_{\oplus,\rm crit} = 2.81 E_{52}^{-1/4} \Delta_{13}^{1/4} \xi_{B,-2} A_*^{5/4} \text{ s}, \quad (24)$$

which is the beginning of our calculation. Since the peak flux of the forward shock emission is comparable to that of the RRS emission, a very early afterglow may be dominated by both of the two regions. An optical flash may even be dominated by the RRS emission if E is very large and A_* is small, which can be estimated by comparing equation (13) with equation (21).

The break frequencies and peak flux for $t_\oplus > T'$ are

$$\begin{aligned} \nu_{\rm m} &= \nu_{\rm m}(T') \left(\frac{t_\oplus}{T'}\right)^{-3/2}, \\ \nu_{\rm c} &= \nu_{\rm c}(T') \left(\frac{t_\oplus}{T'}\right)^{1/2}, \\ F_{\nu,\rm max} &= F_{\nu,\rm max}(T') \left(\frac{t_\oplus}{T'}\right)^{-1/2}. \end{aligned} \quad (25)$$

The self-absorption frequency is: (1) in the fast-cooling phase, $\nu_{\rm a} \propto (t_\oplus/T')^{-2/3}$ for $\nu_{\rm c} \leqslant \nu_{\rm a} \leqslant \nu_{\rm m}$, and $\nu_{\rm a} \propto (t_\oplus/T')^{-8/5}$ for $\nu_{\rm a} \leqslant \nu_{\rm c} \leqslant \nu_{\rm m}$; (2) in the slow-cooling phase, $\nu_{\rm a} \propto (t_\oplus/T')^{-3/5}$ for $\nu_{\rm a} \leqslant \nu_{\rm m} \leqslant \nu_{\rm c}$. The case of $\nu_{\rm m} \leqslant \nu_{\rm a} \leqslant \nu_{\rm c}$ seems impossible before $t'_{\oplus,\rm nr} = 2.763 \times 10^3 E_{52} A_*^{-1} \Delta_{13}^{-1} T'$.

3.3 Light curves of optical and radio afterglows

The above subsections give the spectral profiles and the decay laws of the break frequencies. In this subsection, we will discuss the light curves at some observed frequencies such as $\nu_{\rm opt} = 4 \times 10^{14}$ Hz and $\nu_{\rm rad} = 8.46$ GHz. We calculate the evolution of the flux densities at these two frequencies with fixed parameters of $\xi_{\rm e,0} = 1.0$, $\xi_{B,-2} = 1.0$ and $\Delta_{13} = 0.5$ but with E_{52} varying between 1.0 and 10^2, and A_* varying between 10^{-2} and 1, to investigate the effects of energy and wind intensity. The values of $\xi_{\rm e,0}$ and $\xi_{B,-2}$ are consistent with the afterglow of GRB 970508 (Wijers & Galama 1999; Granot, Piran & Sari 1999) and the optical flash and afterglow of GRB 990123 (Wang, Dai & Lu 2000), and $\Delta_{13} = 0.5$ is consistent with $T' = \Delta/4c \approx 42$ s, which is the peak time of the optical flash of GRB 990123. The light curves in six cases and at two frequencies are shown in Figs 1–6 .

The emission from RRS is nearly comparable to or dominant over that from the forward shock at optical frequency. This is naturally estimated from the ratio of the reverse shocked electron number of

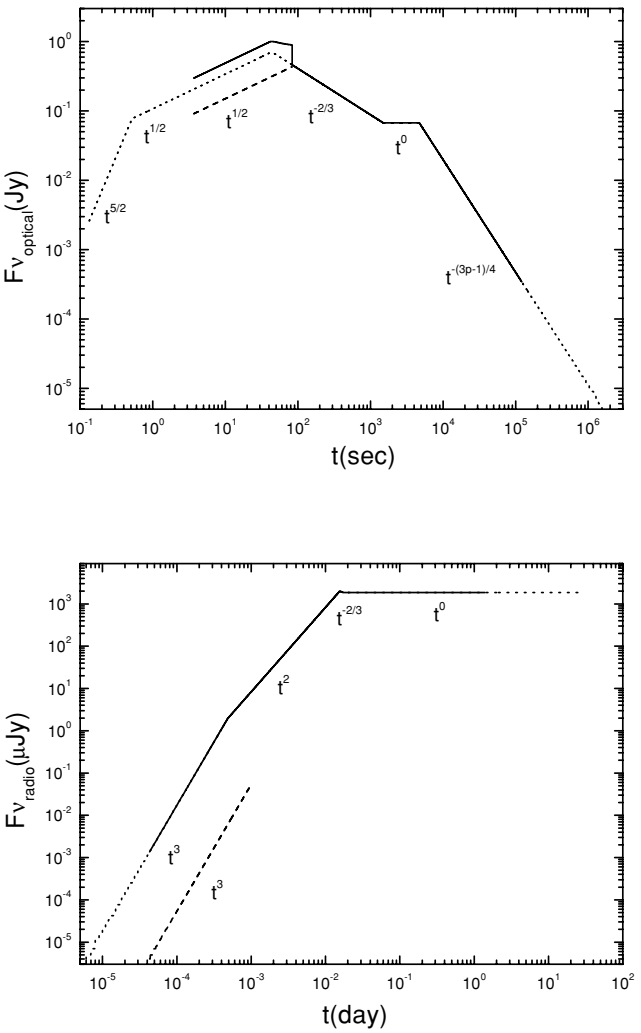

Figure 1. Light curves of very early afterglows in a stellar wind. The upper panel corresponds to optical flashes at $\nu_{\rm opt} = 4 \times 10^{14}$ Hz, and the bottom panel to radio flares at 8.46 GHz. The dashed, dotted and solid lines represent the radiation from the relativistic reverse shock and forward shock and their total emission. $E = 10^{52}$ erg, $A = 3 \times 10^{34}$ cm^{-1}, $\eta = 300$, $\Delta = 5 \times 10^{12}$ cm, $\xi_{\rm e} = 0.6$, $\xi_B = 10^{-2}$, $D = 10^{28}$ cm and $p = 2.5$ are assumed. $t_{\rm co} \approx 856$ s is the time when $\nu_{\rm c} = \nu_{\rm opt}$.

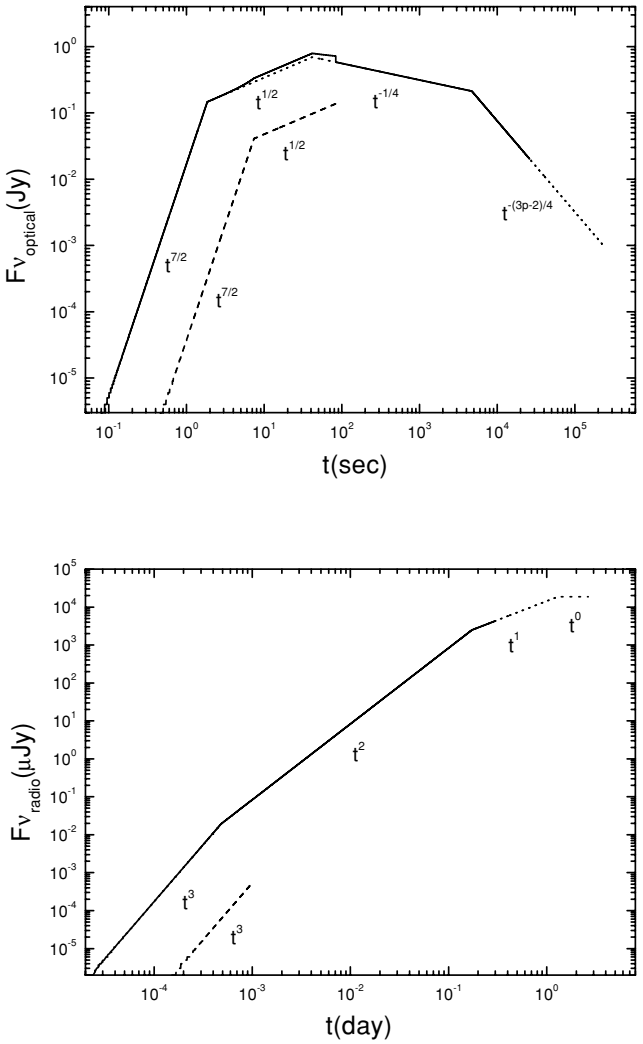

Figure 2. Light curves of very early afterglows in a stellar wind. Same as Fig. 1 except for $E = 10^{52}$ erg, $A = 3 \times 10^{35}$ cm^{-1}.

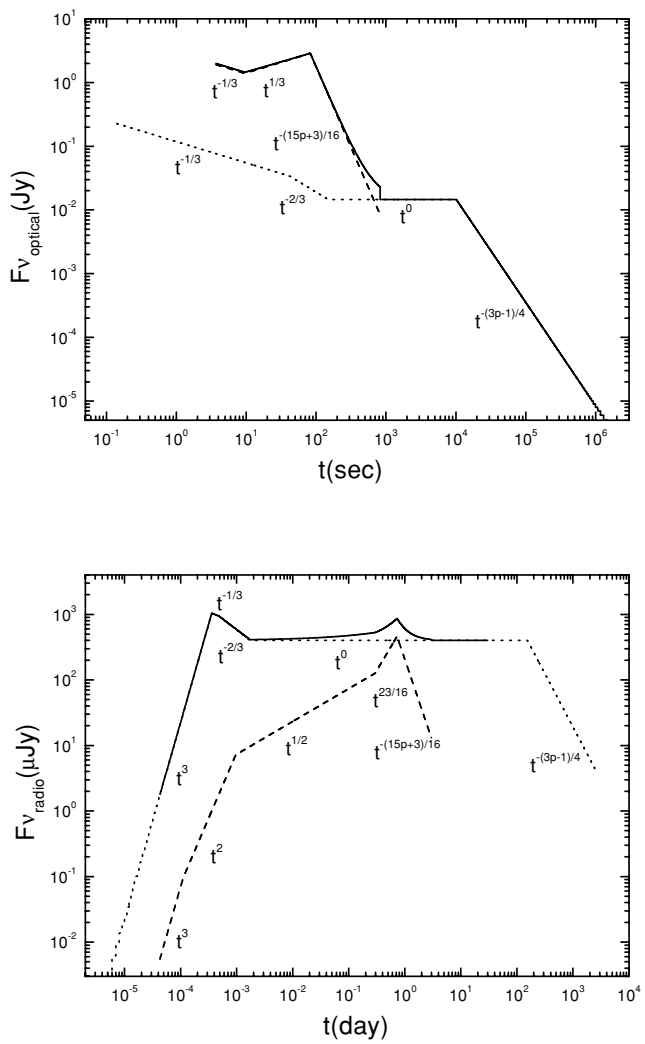

Figure 3. Light curves of very early afterglows in a stellar wind. Same as Fig. 1 except for $E = 10^{53}$ erg, $A = 3 \times 10^{33}$ cm^{-1}.

the shell to the forward shocked electron number,

$$\frac{N_{\rm e,rs}}{N_{\rm e,fs}} = 3f^{1/2} = 4.21E_{52}^{1/2}A_*^{-1/2}\Delta_{13}^{-1/2}\eta_{300}^{-1}, \quad (26)$$

before RRS crosses the shell, compared with equation (58) of Chevalier & Li (2000). In detail, the maximum optical flux in RRS reaches at $t_\oplus = T$,

$$F_{\nu_{\rm opt}}^{\rm rs}(T) = F_{\nu,\max}^{\rm rs}(\nu_{\rm opt}/\nu_{\rm c})^{-1/2} = 8.16 \times 10^{-2}E_{52}^{5/4}\eta_{300}^{-1}A_*^{-1/2}\Delta_{13}^{-3/4}\xi_{B,-2}^{-1/4}D_{28}^{-2}\ {\rm Jy}, \quad (27)$$

when RRS is still in the fast-cooling regime, as emphasized by Chevalier & Li (2000). The above equation is not suitable for the case of $E_{52} = 10$, $A_* = 10^{-2}$, where RRS enters the slow-cooling regime before it crosses the shell, because we can use equations (11) and (12) to get the transition time $t_{\rm mc}^{\rm rs}$ by $\nu_{\rm m} = \nu_{\rm c}$,

$$\frac{t_{\rm mc}^{\rm rs}}{T} = 2.56 \times 10^2 E_{52}^{-1/2}\eta_{300}A_*^{3/2}\Delta_{13}^{-1/2}\xi_{\rm e,0}\xi_{B,-2} = 0.11 < 1, \quad (28)$$

for $E_{52} = 10$, $A_* = 10^{-2}$. The optical flux contributed by the forward shock reaches its maximum at $t_\oplus = T'$,

$$F_{\nu_{\rm opt}}^{\rm fs}(T') = F_{\nu,\max}^{\rm fs}(\nu_{\rm opt}/\nu_{\rm c})^{-1/2} = 0.583E_{52}^{3/4}\Delta_{13}^{-1/4}\xi_{B,-2}^{-3/4}D_{28}^{-2}\ {\rm Jy}, \quad (29)$$

except in the two cases of $E_{52} = 10$, $A_* = 0.1$, and $E_{52} = 10$, $A_* = 10^{-2}$. For these two cases, the optical flux by the forward shock reaches the maximum before RRS has crossed the shell and decays to

$$F_{\nu_{\rm opt}}^{\rm fs}(T') = F_{\nu,\max}^{\rm fs}\left(\frac{\nu_{\rm opt}}{\nu_{\rm c}}\right)^{1/3} = 1.583E_{53}^{1/3}\left(\frac{\Delta_{13}}{0.5}\right)^{-2/3}\left(\frac{A_*}{0.1}\right)^{5/3}\xi_{B,-2}^{1/2}D_{28}^{-2}\ {\rm Jy}. \quad (30)$$

For more energetic fireball and weaker stellar wind, the emission from RRS becomes stronger than that from the forward shock. The weakest RRS case is for $E = 10^{52}$ erg, $A_* = 1.0$, where the forward shock dominates RRS at $\nu_{\rm opt}$ by about one order of magnitude (Fig. 2). The peak flux $F_{\nu_{\rm opt},\rm peak}$ increases with both E and A_* and varies from $\sim$1 to $\sim 10^2$ Jy. An optical flash occurs in all cases, although its properties, such as the brightening and decaying time-scales and the light-curve index, may be different from each other. The time-scale of emission with flux above 1 Jy ranges from 10 to 10^4 s. None of the six cases discussed here is consistent with the

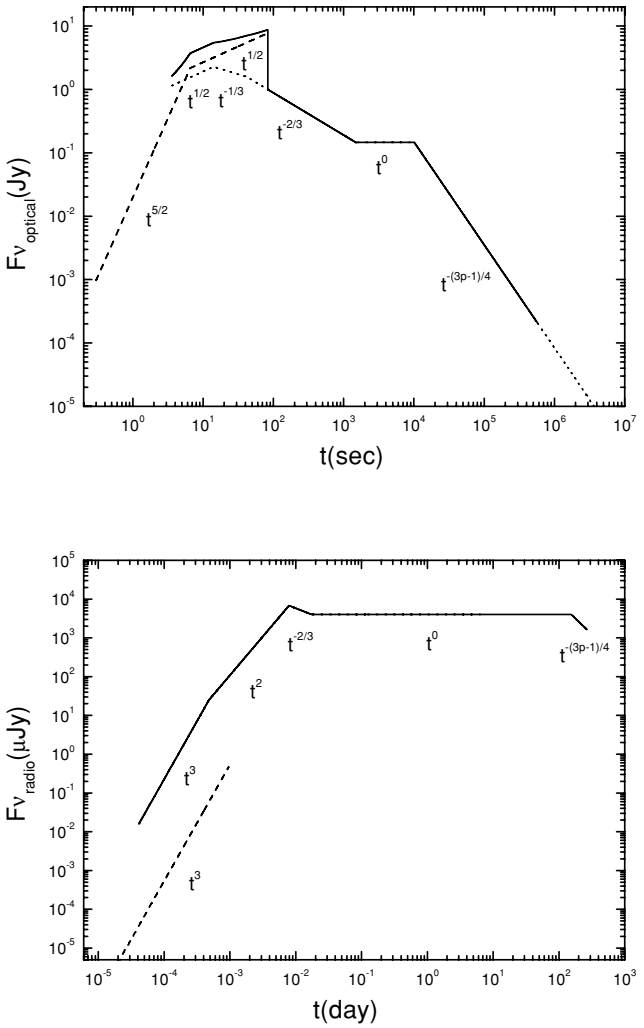

Figure 4. Light curves of very early afterglows in a stellar wind. Same as Fig. 1 except for $E = 10^{53}$ erg, $A = 3 \times 10^{34}$ cm^{-1}.

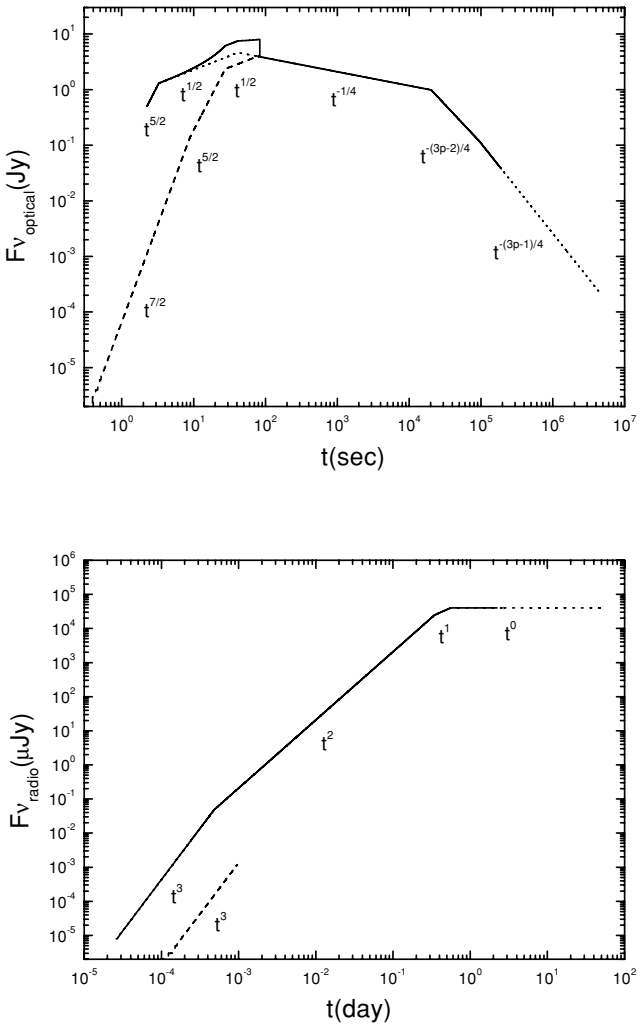

Figure 5. Light curves of very early afterglows in a stellar wind. Same as Fig. 1 except for $E = 10^{53}$ erg, $A = 3 \times 10^{35}$ cm^{-1}.

rapid brightening ($F_{\nu_{\rm opt}} \propto t_{\oplus}^{3.4}$) and fast decay ($\propto t_{\oplus}^{-2.1}$) of the optical flash of GRB 990123. This further confirms the result of Chevalier & Li (2000) that the optical flash of GRB 990123 originates from a homogeneous ISM.

The radio afterglow is mainly attributed to radiation from the forward shock and we can neglect the contribution of the emission from RRS. The light-curve indices of the forward shock are 2, $-2/3$, *0* and $-(3p-1)/4$ from low to high frequencies in Figs 1 , 4 and 6, as shown in Chevalier & Li (2000). We also get an index $\beta = 3$, which does not equal the 7/4 of Chevalier & Li (2000) at very early times. Indices of 2, 1 and 0 in Figs 2 and 5 are consistent with the results of Chevalier & Li (2000). The peak flux at radio band varies by two orders of magnitude, from 10^3 to 10^5 μJy. There is a long-lasting platform in the radio flux before the forward shock enters the non-relativistic phase (see also fig. 3 of Panaitescu & Kumar 2000). It might be used to distinguish the wind environment from the uniform ISM environment of GRBs and give further hints on the central engine.

4 SUMMARY

We have analysed very early afterglows in wind environments by considering the radiation from both a relativistic reverse shock and a relativistic forward shock. The resulting optical flash in the wind case is mainly attributed to RRS because of reduction of the flux from the forward shock by synchrotron self-absorption. For more energetic fireball and weaker stellar wind, the optical emission from RRS becomes stronger than that from the forward shock. The resulting radio flare is largely produced by the forward shock emission.

Theoretically, the peak flux of the optical flash ranges from 1 to 10^2 Jy, and the peak time since the GRB trigger is tens of seconds, which is determined by the shell width. In our cases we choose the width according to the typical time-scales of long γ-ray bursts, i.e. of the order of a few tens of seconds. Such a large optical flux at very early times is due to the dense wind at small radius. If optical observations could be done in a few seconds after the GRB trigger, then one could discriminate the wind environment from the uniform ISM environment. This is a challenge for current observational instruments. While strong optical flashes have been predicted theoretically in this research as well as by many other authors, in realistic observations optical flash has so far been observed only from GRB 990123. The missing of a significant number of strong optical flashes has been interpreted as due to dust obscuration Soderberg & Ramirez-Ruiz (2002a,b). We propose that a further contribution to the reduction of the optical flash may come from the dense shell

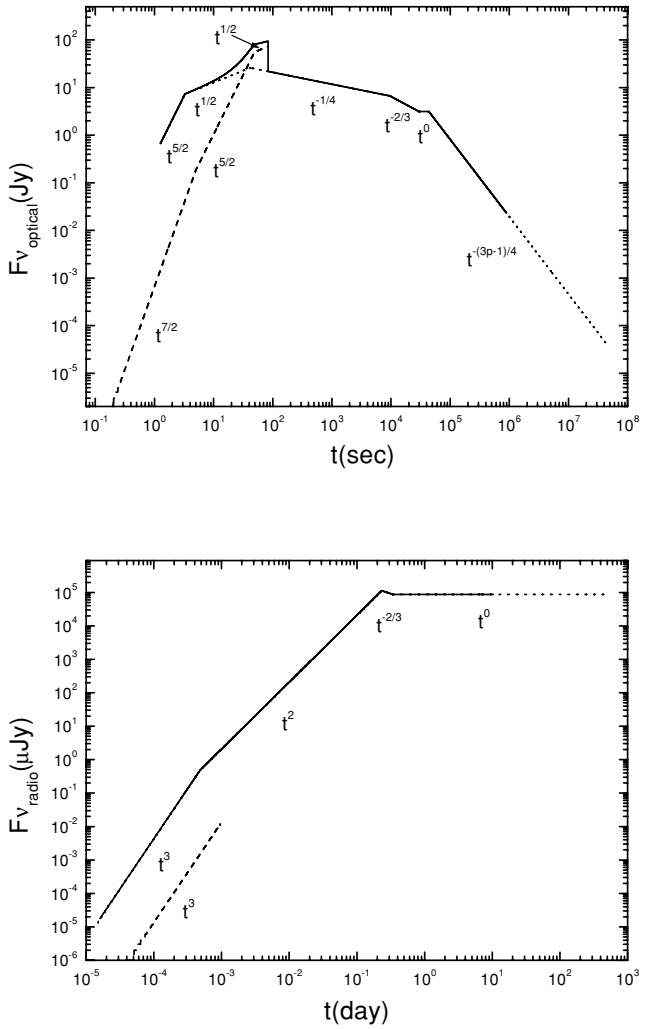

Figure 6. Light curves of very early afterglows in a stellar wind. Same as Fig. 1 except for $E = 10^{54}$ erg, $A = 3 \times 10^{35}$ cm^{-1}.

around the stellar wind with column density about 10^{20}–10^{21} cm^{-2} (Ramirez-Ruiz et al. 2001). Another characteristic of wind environment that might be easier for observations is a long-lasting platform in radio flux, which arises from the interaction of the forward shock with the wind matter.

However, dust extinction could not darken a fourth-magnitude ($\sim$100 Jy) optical flash significantly to be immune to the optical survey. The non-detections of optical flashes brighter than about ninth magnitude would eventually constrain the isotropic energies of GRBs to be no more than a few 10^{52} erg and result in relatively weak circum-burst wind intensities with $A_* < 1.0$, according to equations (13), (21) and (27). We expect future observations on early afterglows to diagnose the environments of GRBs efficiently.

ACKNOWLEDGMENTS

We wish to thank the referee for valuable suggestions. XFW would like to thank D. M. Wei, X. Y. Wang, Z. Li, Y. Z. Fan and J. B. Feng for fruitful discussions. This work was supported by the National Natural Science Foundation of China (grants numbers 19973003, 10233010, 10003001), the National 973 project (NKBRSF G19990754), the Foundation for the Authors of National Excellent Doctoral Dissertations of P.R. China (Project No. 200125) and the Special Funds for Major State Basic Research Projects.

REFERENCES

Akerlof C. W. et al., 1999, Nat, 398, 400
Ballantyne D., Ramirez-Ruiz E., 2001, ApJ, 559, L83
Blandford R. D., McKee C. F., 1976, Phys. Fluids, 19, 1130 (BM)
Bloom J. S. et al., 1999, Nat, 401, 453
Bloom J. S. et al., 2002, ApJ, 572, L45
Böttcher M., Fryer C. L., 2001, ApJ, 547, 338
Castro-Tirado A. J. et al., 2001, A&A, 370, 398
Chevalier R. A., Li Z. Y., 1999, ApJ, 520, L29
Chevalier R. A., Li Z. Y., 2000, ApJ, 536, 195
Dai Z. G., Gou L. J., 2001, ApJ, 552, 72
Dai Z. G., Lu T., 2001, ApJ, 551, 249
Dai Z. G., Lu T., 1998, MNRAS, 298, 87
Frail D. A. et al., 2000, ApJ, 534, 559
Galama T. J. et al., 1998, Nat, 395, 670
Gou L. J., Dai Z. G., Huang Y. F., Lu T., 2001, A&A, 368, 464
Granot J., Piran T., Sari R., 1999, ApJ, 527, 236
Huang Y. F., Dai Z. G., Lu T., 1998, A&A, 336, L69
Huang Y. F., Dai Z. G., Lu T., 1999, MNRAS, 309, 513
Huang Y. F., Dai Z. G., Lu T., 2000, MNRAS, 316, 943
Kobayashi S., 2000, ApJ, 545, 807
Kobayashi S., Sari R., 2000, ApJ, 542, 819
Lazzati D., Perna R., 2002, MNRAS, 330, 383
Lazzati D. et al., 2001, A&A, 378, 996
Li Z. Y., Chevalier R. A., 1999, ApJ, 526, 716
Li Z. Y., Chevalier R. A., 2001, ApJ, 551, 940
Livio M., Waxman E., 2000, ApJ, 538, 187
McLaughlin G. C., Wijers R. A. M. J., Brown G. E., Bethe H. A., 2002, ApJ, 567, 454
Mészásros P., 2002, ARA&A, 40, 137
Mészáros P., Rees M. J., 1997, ApJ, 476, 232
Mészáros P., Rees M. J., 1999, MNRAS, 306, L39
Mészáros P., Rees M. J., 2001, ApJ, 556, L37
Paczyński B., 1998, ApJ, 494, L45
Panaitescu A., 2001, ApJ, 556, 1002
Panaitescu A., Kumar P., 2000, ApJ, 543, 66
Panaitescu A., Kumar P., 2001, ApJ, 554, 667
Panaitescu A., Kumar P., 2002, ApJ, 571, 779
Piran T., 1999, Phys. Rep., 314, 575
Ramirez-Ruiz E., Dray L. M., Madau P., Tout C. A., 2001, MNRAS, 327, 829
Rees M. J., Mészáros P., 2000, ApJ, 545, L73
Reeves J. N. et al., 2002, Nat, 416, 512
Reichart D. E., 1999, ApJ, 521, L111
Rybicki G. B., Lightman A. P., 1979, Radiative Processes in Astrophysics. Wiley, New York
Sahu K. C. et al., 2000, ApJ, 540, 74
Sari R., Piran T., 1995, ApJ, 455, L143
Sari R., Piran T., 1999a, ApJ, 520, 641
Sari R., Piran T., 1999b, ApJ, 517, L109
Sari R., Piran T., Narayan R., 1998, ApJ, 497, L17
Scalo J., Wheeler J. C., 2001, ApJ, 562, 664
Soderberg A. M., Ramirez-Ruiz E., 2002a, MNRAS, 330, L24
Soderberg A. M., Ramirez-Ruiz E., 2002b, MNRAS, submitted (astro-ph/0210524)
Sokolov V. V., 2001, Bull. Special Astrophys. Obser. Russian Astron. Soc., 50 (astro-ph/0107399)
van Paradijs J., Kouveliotou C., Wijers R. A. M. J., 2000, ARA&A, 38, 379
Vietri M., Ghisellini G., Lazzati D., Fiore F., Stella L., 2001, ApJ, 550, L43
Wang X. Y., Dai Z. G., Lu T., 2000, MNRAS, 319, 1159
Wijers R. A. M. J., Rees M. J., Mészáros P., 1997, MNRAS, 288, L51
Wijers R. A. M. J., Galama T. J., 1999, ApJ, 523, 177
Woosley S. E., 1993, ApJ, 405, 273

APPENDIX A: SYNCHROTRON SELF- ABSORPTION BY ELECTRONS WITH A BROKEN POWER-LAW DISTRIBUTION

A1 Synchrotron self-absorption coefficient by electrons with one single power-law distribution

All the quantities below are in the comoving reference frame. The power-law distribution of the shock-accelerated electrons can be written as $N(\gamma_e)d\gamma_e = N_{\gamma_e}\gamma_e^{-p}d\gamma_e$, where N_{γ_e} is the normalized coefficient and $\gamma_1 \leqslant \gamma_e \leqslant \gamma_2$. The power radiated from an electron with γ_e is (Rybicki & Lightman 1979)

$$P(\nu, \gamma_e) = \frac{2\pi\sqrt{3}q_e^2\nu_L \sin\theta}{c}\frac{\nu}{\nu_c}\int_{\nu/\nu_c}^{\infty} K_{5/3}(t)\,dt, \tag{A1}$$

where $\nu_L = q_e\ B\ /2\pi\ m_e\ c$ is the Larmor frequency and $\nu_c = (3\gamma^2{}_e\nu_L \sin\theta)/2$ is the typical frequency emitted by this electron. We rewrite the self-absorption coefficient of equation (6.52) of Rybicki & Lightman (1979), and get

$$k_\nu = -\frac{1}{8\pi m_e\nu^2}\int_{\gamma_1}^{\gamma_2} P(\nu, \gamma_e)\gamma_e^2\frac{d}{d\gamma_e}\left[\frac{N(\gamma_e)}{\gamma_e^2}\right]d\gamma_e. \tag{A2}$$

Before integrating the above equation, we define $\nu_1 = (3\gamma_1^2\,\nu_L \sin)/2$ and $\nu_2 = (3\gamma_2^2\ \nu_L \sin\theta)/2$. For $\nu \ll \nu_1$, we have

$$k_\nu = \frac{\pi^{1/3}}{2^{2/3}3^{1/3}\Gamma(\frac{1}{3})}\frac{p+2}{p+\frac{2}{3}}\frac{q_e^{8/3}}{(m_e c)^{5/3}} \times N_{\gamma_e}B^{2/3}(\sin\theta)^{2/3}\gamma_1^{-(p+2/3)}\nu^{-5/3}. \tag{A3}$$

For simplicity, we take an isotropic distribution of θ with

$$\langle(\sin\theta)^{2/3}\rangle = \frac{\sqrt{\pi}\Gamma(\frac{1}{3})}{5\Gamma(\frac{5}{6})}$$

and obtain

$$k_\nu = 114.65\frac{p+2}{p+\frac{2}{3}}N_{\gamma_e}B^{2/3}\gamma_1^{-(p+2/3)}\nu^{-5/3}. \tag{A4}$$

For $\nu_1 \ll \nu \ll \nu_2$, we obtain

$$k_\nu = g(p)\frac{q_e^3}{2\pi m_e}\left(\frac{3q_e}{2\pi m_e^3c^5}\right)^{p/2}(m_e c^2)^{p-1} \times N_{\gamma_e}B^{(p+2)/2}(\sin\theta)^{(p+2)/2}\nu^{-(p+4)/2}, \tag{A5}$$

where

$$g(p) = \frac{\sqrt{3}}{16}\Gamma\left(\frac{3p+2}{12}\right)\Gamma\left(\frac{3p+10}{12}\right)\left(p+\frac{10}{3}\right).$$

This case is the same as the well-known equation (6.53) of Rybicki & Lightman (1979). For $\nu_2 \ll \nu$, we get

$$k_\nu = \frac{\sqrt{3}\pi^{3/2}}{9\sqrt{2}}\frac{(p+2)}{\sin\theta}N_{\gamma_e}\gamma_2^{-(p+4)}\frac{q_e}{B}\left(\frac{\nu}{\nu_2}\right)^{-5/2}e^{-\nu/\nu_2}, \tag{A6}$$

and if we take the isotropic distribution $\langle\sin\theta\rangle = 1/4$,

$$k_\nu = \frac{2\sqrt{6}\pi^{3/2}}{9}(p+2)N_{\gamma_e}\gamma_2^{-(p+4)}\frac{q_e}{B}\left(\frac{\nu}{\nu_2}\right)^{-5/2}e^{-\nu/\nu_2}, \tag{A7}$$

which is always neglected in astrophysics but it may be applied for GRBs in which the self-absorption $\nu_a > \nu_2$ is possible and it may explain the spectrum of GRBs combining inverse Compton scattering.

For unification and convenience for comparison in the next section, we rewrite equations (A3), (A5) and (A7),

$$k_\nu = c_1\frac{q_e}{B}N_{\gamma_e}\gamma_1^{-(p+4)}\left(\frac{\nu}{\nu_1}\right)^{-5/3}, \qquad \nu \ll \nu_1, \tag{A8}$$

$$k_\nu = c_2\frac{q_e}{B}N_{\gamma_e}\gamma_1^{-(p+4)}\left(\frac{\nu}{\nu_1}\right)^{-(p+4)/2}, \quad \nu_1 \ll \nu \ll \nu_2, \tag{A9}$$

$$k_\nu = c_3\frac{q_e}{B}N_{\gamma_e}\gamma_2^{-(p+4)}\left(\frac{\nu}{\nu_2}\right)^{-5/2}e^{-\nu/\nu_2}, \quad \nu_2 \ll \nu, \tag{A10}$$

where

$$c_1 = \frac{32\pi^2}{9\times 2^{1/3}\Gamma(\frac{1}{3})}\frac{p+2}{p+\frac{2}{3}},$$

$$c_2 = \frac{32\pi}{9}2^{p/2}g(p),$$

$$c_3 = \frac{2\sqrt{6}\pi^{3/2}}{9}(p+2),$$

which are of the same order. For illustration, $c_1 = 14.78$, $c_2 = 17.80$ and $c_3 = 13.64$ for $p = 2.5$; and $c_1 = 15.60$, $c_2 = 15.64$ and $c_3 = 12.12$ for $p = 2.0$. So the above expression for k_ν still is valid even when ν approaches ν_1 or ν_2. For simulations, the discontinuity of k_ν can be removed if we constrain $c_1 = c_2 = c_3/$ e.

A2 Self-absorption frequency and the spectra of fast- and slow-cooling cases

Now we consider the absorption by electrons with a broken power-law distribution. The break Lorentz factors are $\gamma_1 < \gamma_2 < \gamma_3$ with power-law indices p_1 of (γ_1, γ_2) (hereafter we refer to this region as region A) and p_2 of (γ_2, γ_3) (region B). For slow cooling $p_1 = -p$ and $p_2 = -(p+1)$ with $\gamma_1 = \gamma_m$, $\gamma_2 = \gamma_c$ and $\gamma_3 = \gamma_M$. For fast cooling $p_1 = -2$ and $p_2 = -(p+1)$ with $\gamma_1 = \gamma_c$, $\gamma_2 = \gamma_m$ and $\gamma_3 = \gamma_M$. Both regions A and B contribute to k_ν. According to equations (A8), (A9) and (A10), we find that k_ν is mainly determined by a nearer region with respect to its frequency ν, i.e. $k_\nu = k_\nu($ A) for $\nu \leqslant \nu_1$ and $\nu_1 < \nu < \nu_2$, while $k_\nu = k_\nu($ B) for $\nu_2 < \nu \leqslant \nu_3$ and $\nu_3 < \nu$.

The self-absorption frequency ν_a is determined by $k_{\nu_a}L \approx 1$, where L is the length of the radiation region in the comoving frame. The spectrum below ν_a will be corrected since the optical depth is larger than unity and $I_\nu \propto j_\nu/k_\nu$. From the above analysis, we obtain the complete spectrum in all cases.

In the fast-cooling phase: (1) for $\nu_a < \nu_c < \nu_m$ the spectral indices of four segments are $(2, 1/3, -1/2, -p/2)$; (2) for $\nu_c < \nu_a < \nu_m$ the spectral indices are $(2, 5/2, -1/2, -p/2)$; (3) for $\nu_c < \nu_m < \nu_a(< \nu_M)$ the spectral indices are $(2, 5/2, 5/2, -p/2)$. Case (3) has rarely been discussed previously in astrophysics and maybe contributes to GRBs but not to their afterglows. There is still case (4) $\nu_M < \nu_a$. We do not discuss it since the flux of $\nu > \nu_M$ is negligible.

In the slow-cooling phase: (1) for $\nu_a < \nu_m < \nu_c\ (<\nu_M)$ we find the spectral indices are $(2, 1/3, -(p-1)/2, -p/2)$; (2) for $\nu_m < \nu_a < \nu_c\ (<\nu_M)$ the spectral indices are $(2, 5/2, -(p-1)/2, -p/2)$; (3) for $\nu_m < \nu_c < \nu_a\ (<\nu_M)$ the spectral indices are $(2, 5/2, 5/2, -p/2)$. For case (1), from equation (A4) we can find ν_a in the observer's frame is consistent with equation (22) of Wijers & Galama (1999), or we use equation (A8) to get the same ν_a as equation (52) ($\nu < \nu_p$) of Panaitescu & Kumar (2000), if we take $N_{\gamma_e} \simeq (p-1)n_e\gamma_m^{p-1}$ and n_e is the electron density in the comoving frame.

This paper has been typeset from a TEX/LATEX file prepared by the author.